

Momentum transport and plasma rotation spin up in TCV

A. Scarabosio, A. Bortolon, B.P. Duval, A. Karpushov, A. Pochelon.

Centre de Recherches en Physique des Plasmas,

Association EURATOM-Confédération Suisse, CRPP EPFL, CH-1015 Lausanne, Switzerland

This paper reports on the experimental observation of toroidal rotation braking and plasma spin up due to the growth and decay of Magnetohydrodynamic (MHD) modes in the Tokamak à Configuration Variable (TCV) operated in the ohmic regime. The results of numerical simulations of momentum spin up, with the goal of evaluating the momentum diffusion coefficient D_ϕ , are also presented. Unlike most experimental studies of momentum transport no external momentum source is applied so the observed rotation is entirely generated by the plasma itself by some transport mechanism such as collisions or turbulence. The ion impurity toroidal velocity is measured via active Charge eXchange Recombination Spectroscopy (CXRS) along the equatorial plane of the vacuum vessel [1] with a temporal resolution of $50 \div 100$ ms and a spatial resolution of 2.5 cm. The MHD activity is monitored with Mirnov magnetic coil arrays and several fast soft X-ray detector arrays.

Ion momentum losses with large MHD

In steady state Ohmic TCV plasmas, the ion rotation velocity generally flows in the direction opposite to the plasma current (counter-current, negative for positive I_p). The profile monotonically increases up to the sawtooth inversion radius, r_{inv} , is stationary at the edge, and flat or hollow inside r_{inv} [1]. In this work, we consider non steady-state plasmas with large persistent MHD os-

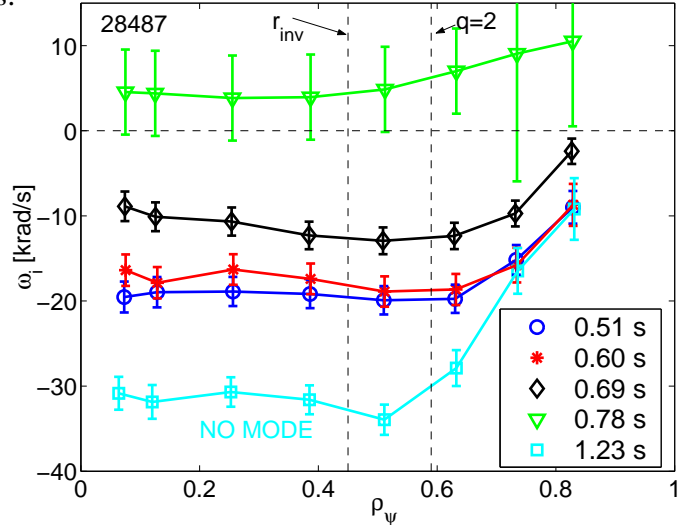


Figure 1: *Evolution of the toroidal rotation profile in the presence of a large magnetic island. The rotation in absence of mode is also shown for comparison (cyan color)*

illations or stronger disruptive instabilities. The presence of MHD modes are observed to flatten the ion toroidal rotation profile over the central region, out to the rational surface of the corresponding mode. Fig. 1 plots the evolution of the ion toroidal angular velocity, $\omega_i = v_\phi/R$, in the presence of a quasi-stationary mode that slows in frequency eventually locking to the vacuum vessel.

The rotation profile that is observed in the absence of the magnetic island is also shown. The temporal evolution of the instability from the magnetic and central SXR signals is shown in figure 2. The phase difference in the magnetic coils shows a $m/n=2/1$ mode structure with an island width of about 7 cm estimated from the soft-X-ray emissivity at $t=0.5$ s. The flat region of the rotation profile extends well outside the magnetic island. While slowing down, the MHD mode presence reduces the central ion rotation to its rotation frequency. As shown in fig. 3, the rotation frequency at the $q=2$ rational surface agrees, within the error, with the mode frequency from the Mirnov coils.

The MHD mode also appears to shift the whole rotation profile while retaining the same gradient outside the rational surface as suggested by the comparison of the black (diamond marker) and red (asterisk marker) profiles in fig. 1. The presence of the instability may thus induce, for a sufficiently low mode frequency, a rotation inversion. This is visible in a similar discharge with the CXRS observation chord observing the plasma edge shown in figure 4. Here the presence of the mode induces a rotation inversion at about $\rho = 0.85$ with considerable edge co-current rotation while the steady state plasma, in absence of the mode, has zero toroidal rotation at the edge. We may conclude that the MHD mode induces a net loss of total momentum in the plasma first reducing the natural rotation frequency of the flux surface where the mode is resonant and then making the central plasma rotate at this frequency. This evolution implies a mechanism that strongly couples the ion fluid with the MHD mode. Usually, when the magnetic island is still rotating at finite frequency, the plasma undergoes a minor disruption. This abrupt instability almost completely brakes the plasma rotation except at the plasma edge where some co-current rotation persists (green profile in figure 1). It should be noted that, in this rapidly evolving plasma, the CX rotation measurement are susceptible to much increased errors due to the rapid variation of the background CX emission (see [1] for details). The toroidal acceleration, or spin-up following the decay of an MHD mode, is considered in the next section.

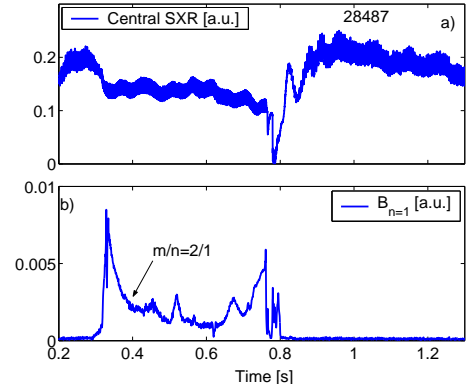


Figure 2: *a) Time trace of central SXR emission, b) $n=1$ component of the edge magnetic signal showing mode amplitude evolution*

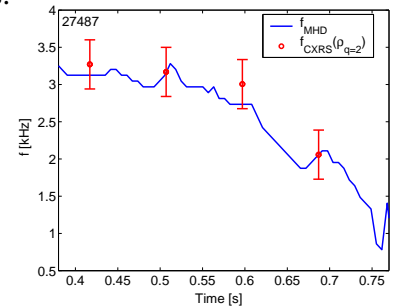


Figure 3: *Comparison of the ion rotation frequency and the MHD mode frequency during mode locking*

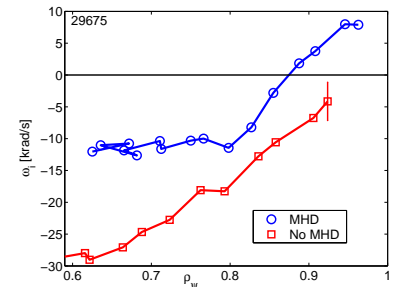


Figure 4: *Comparison of edge rotation profiles with and without MHD mode*

Toroidal rotation spin-up

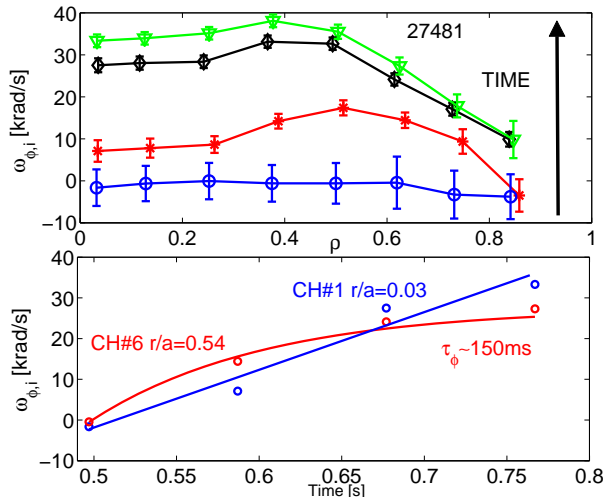


Figure 5: a) Spin-up of the toroidal rotation, b) Details of the temporal evolution region may be the effect of the central sawtooth activity, which reappears early after the minor disruption. An example of such an evolution is shown in figure 5 and analysed in detail in the next section.

Momentum transport modelling

The time evolution of the velocity profiles has been simulated with a 1D momentum transport model of the form:

$$\frac{\partial P}{\partial t} = \nabla \cdot \Gamma_{r\phi} + S_\phi \quad (1)$$

$$\Gamma_{r\phi} = D_\phi \frac{\partial P}{\partial r} + v_c \frac{r}{a} P + D_\phi \frac{\alpha n_i m_i}{e B_\theta} \frac{1}{\sqrt{\epsilon}} \frac{1}{r} \frac{\partial T_i}{\partial r} \quad (2)$$

where $P = n_i m_i v_\phi$, $\Gamma_{r\phi}$ is the radial angular momentum flux, S_ϕ is an edge localised momentum source, ϵ is the inverse aspect ratio, a is the minor radius and α is a numerical constant. The first term in (2) represents the momentum diffusion arising from the ion viscosity, the second a convective contribution to the flux and the third a simplified form of the neoclassical momentum source arising from the non-diagonal part of the transport matrix calculated in [2]. The initial condition is taken from the experiment and the boundary condition at the edge, $v_\phi(a,t)$, is reduced to zero exponentially with a characteristic time of $\tau_\phi = 150$ ms, consistent with the experimental observation. D_ϕ , v_c , α and S_ϕ are used as free parameters to be fitted to the experimental data in the least square sense. The diffusion coefficient is proportional to the neoclassical value [2] $D_\phi = \beta D_{neo}$ with $D_{neo} = 0.1 v_{ii} \rho_L^2$ where v_{ii} is the ion collision frequency and ρ_L is ion Larmor radius. D_{neo} typically ranges from $0.003 \text{ m}^2/\text{s}^2$ at the plasma centre to $0.015 \text{ m}^2/\text{s}^2$ at the edge. To approximately account for the effect of the sawtooth activity, which flattens the

The toroidal rotation profiles evolve on a slower time scale than other main plasma parameters such as electron density and temperatures. These profiles attain a stationary value in less than 90ms while the rotation profile is still evolving. An analysis of the, relatively limited, time evolution of the CX velocities shows a growth with a characteristic time constant in the range of $\tau_\phi = 100 \div 150$ ms in the radial region outside the inversion radius.

The more linear growth in the central plasma

region may be the effect of the central sawtooth activity, which reappears early after the minor disruption. An example of such an evolution is shown in figure 5 and analysed in detail in the next section.

source model	D/D_{neo}	v_c	α	S_ϕ
distributed	12 (best-fit)	0 (fixed)	-1.2 (best-fit)	0 (fixed)
edge localized	40 (best-fit)	3.4 m/s (best-fit)	0 (fixed)	$6.5 \cdot 10^4 m/s^2$ (best-fit)

Table 1: Summary of the source models and best-fit results

central profile, only the diffusive part of the radial momentum flux (2) is retained inside r_{inv} . Density gradients are neglected. We consider here two source models. The first employs the neoclassical distributed momentum source (2nd term in eq. 2) with no convective term (3rd term).

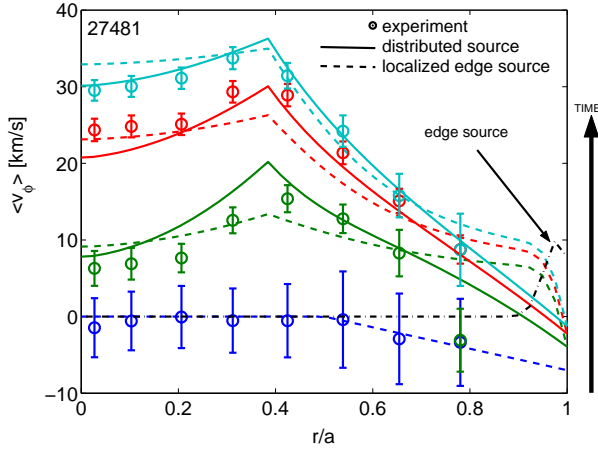


Figure 6: Comparison of different model of the momentum spin-up (full line: distributed source, dash line: edge localized source) with the experiment (points).

The simulation is quite satisfactory for both models for the plasma core. Only the outermost measurement significantly differs in the simulations. Due to large uncertainties and poor edge temporal and spatial resolution it is not possible to establish which is the most appropriate source model, although, given the low steady-state observed edge rotation the localised edge source model would not be appropriate for TCV ohmic plasmas. The best-fit coefficient $\alpha \sim -1.2$ of the neoclassical flux has same sign and order of magnitude as that calculated by Rosenbluth ($\alpha = -3.5$). The almost four times higher diffusion coefficient required for the edge source model may be explained by considering that the same momentum must diffuse through a larger portion of plasma to reach the centre. A non negligible inward pinch of 3.4 m/s is needed to reproduce the experimental peaking. In all conditions the momentum diffusion coefficient, D_ϕ , is found to be much larger than neoclassical indicating anomalous momentum transport in TCV Ohmic plasmas. *This work was partly supported by the Swiss National Science Foundation.*

References

- [1] A. Bortolon et al. this conference.
- [2] M. N. Rosenbluth et al., in Plasma Physics and Controlled Fusion Research (IAEA, Vienna 1971), Vol. I, p. 485.
- [3] W. D Lee et al., Phys. Rev. Letters, Vol. 91, No. 20, 2003

Equation 1 then reproduces the neoclassical momentum diffusion equation derived from kinetic theory by Rosenbluth in [2]. The second model explores a situation where the momentum source is located at the plasma edge, possibly generated by edge turbulence, with the momentum diffusing to the plasma centre. An inward pinch term is used to reproduce the profile peaking. This kind of scenario has been sometimes invoked to explain the spin up during the L-H transition [3]. The models and the best-fit results are summarised in table 1 and figure 6.